iScience

CellPress
OPEN ACCESS

Article

Frequency-specific segregation and integration of human cerebral cortex: An intrinsic functional atlas

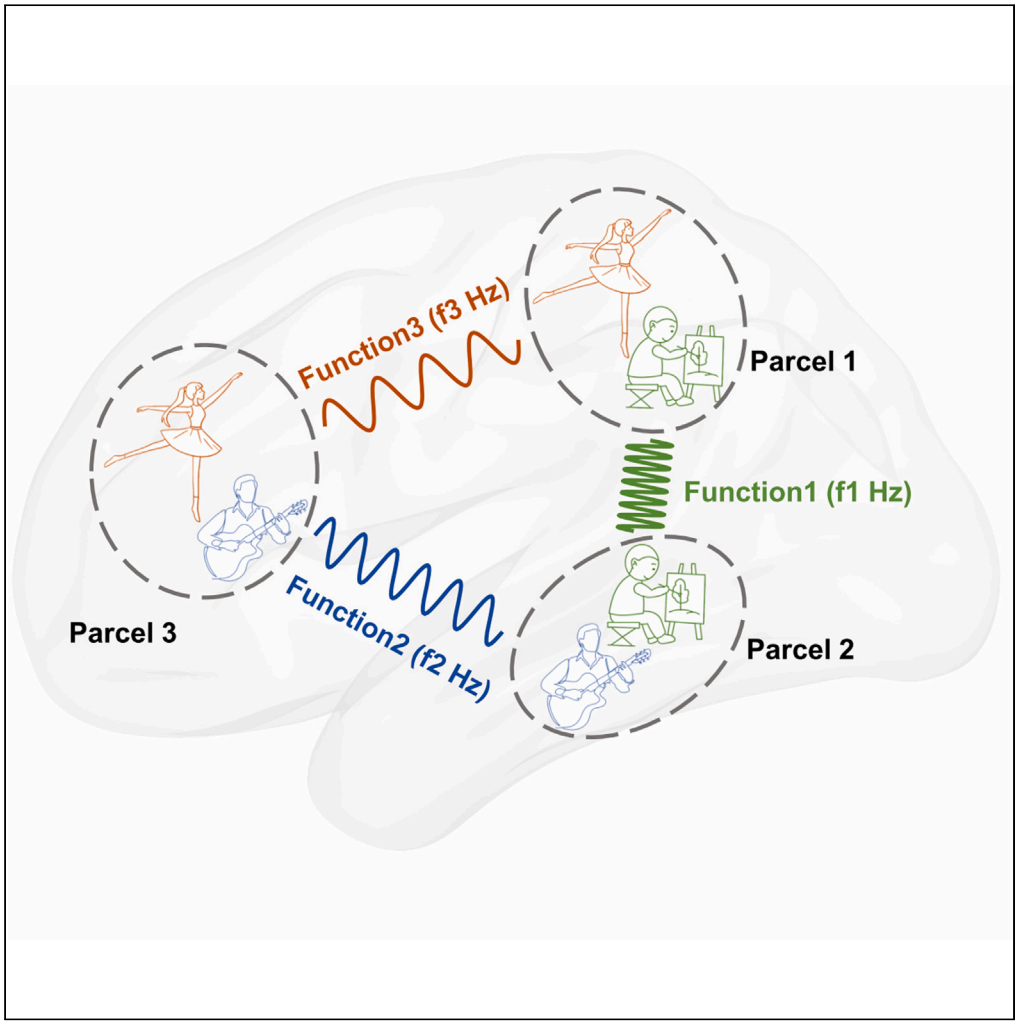

Zhiguo Luo, Erwei Yin, Ling-Li Zeng, ..., Limin Peng, Ye Yan, Dewen Hu

dwhu@nudt.edu.cn

Highlights

Functional parcellation of the human cerebral cortex is frequency specific

A single cortical parcel may communicate with other parcels through different frequency bands

There is a cognitive control system additionally from a frequency perspective

Luo et al., iScience 27, 109206
March 15, 2024
https://doi.org/10.1016/j.isci.2024.109206

iScience

CellPress
OPEN ACCESS

Article

Frequency-specific segregation and integration of human cerebral cortex: An intrinsic functional atlas

Zhiguo Luo,[1,2,3] Erwei Yin,[2,3] Ling-Li Zeng,[1] Hui Shen,[1] Jianpo Su,[1] Limin Peng,[1] Ye Yan,[2,3] and Dewen Hu[1,4,*]

SUMMARY

The cognitive and behavioral functions of the human brain are supported by its frequency multiplexing mechanism. However, there is limited understanding of the dynamics of the functional network topology. This study aims to investigate the frequency-specific topology of the functional human brain using 7T rs-fMRI data. Frequency-specific parcellations were first performed, revealing frequency-dependent dynamics within the frontoparietal control, parietal memory, and visual networks. An intrinsic functional atlas containing 456 parcels was proposed and validated using stereo-EEG. Graph theory analysis suggested that, in addition to the task-positive vs. task-negative organization observed in static networks, there was a cognitive control system additionally from a frequency perspective. The reproducibility and plausibility of the identified hub sets were confirmed through 3T fMRI analysis, and their artificial removal had distinct effects on network topology. These results indicate a more intricate and subtle dynamics of the functional human brain and emphasize the significance of accurate topography.

INTRODUCTION

Modeling functional brain networks is essential to explain brain cognition, behavior, and disease. A growing number of studies have explored functional human brain using fMRI for that it can enable non-invasive imaging with well-balanced spatial and temporal resolution.[1]

Topography and topology analysis based on resting-state functional connectivity play crucial roles in brain network modeling. Topography analysis, whose primary current method is parcellation, tries to identify brain structure at various spatial scales (networks or brain regions). Several studies have parcellated the functional human brain via (1) grouping units with similar functional connectivity (FC) patterns by unsupervised clustering[2–5] or matrix factorization[6]; or (2) identifying boundaries with abrupt FC changes.[7,8] Topology analysis mainly quantifies the segregation and integration of neural information using graph theory methods.[9] The concepts in the following section demonstrate the relationship between topology and topography: communities (networks) are assemblages of nodes (brain areas) and edges (connectivities). Studies suggest that certain nodes called connector hubs promote communication between networks.[10–12]

Benefitting from the high temporal resolution, electroencephalography (EEG) and magnetoencephalography (MEG) studies have widely reported the frequency-dependent spontaneous synchronized brain activities at >1 Hz. For instance, Hillebrand et al.[13] observe opposite directions of information flow in the high- (α1, α2, and β) and low (θ)-frequency bands using MEG data. Brookes et al.[14] get MEG-derived resting-state networks (RSNs) using independent component analysis in α and β band and found them significantly similar in spatial structure compared with RSNs derived from fMRI. Hipp et al.[15] reveal that MEG global connectivities are spatially symmetric and depended on the underlying carrier frequency. Li et al.[16] propose an emotion recognition model achieving an accuracy of 84.56% by learning discriminative graph topologies in EEG brain networks in θ, α, β, and γ bands. van Lutterveld et al.[17] find that experienced meditators have better integrated EEG functional network topology in α band during meditation. However, suffering from the volume conduction effect of the human skull and the poor spatial resolution, both EEG and MEG often play supportive roles for resting-state fMRI (rs-fMRI) in exploring cortical networking mechanism by providing direct electrophysiological evidence.[18]

Although fMRI captures ultra-slow (<1 Hz) neural oscillations indirectly through hemodynamics, stationarity assumption has been proved to be too simplistic to describe resting-state brain activity in this frequency band.[19] Buzsáki and Draguhn indicate that the log power of brain oscillations decreases nearly linearly with increasing log frequency,[20] and Shafiei et al. find that rs-fMRI connectivity patterns can be predicted from band-limited MEG FC via a multilinear regression model, indicating that neural signals captured by fMRI contain effective frequency-specific components.[21] Nonstationary of the resting-state human brain has been widely reported in fMRI studies from dynamic[5,22] or frequency[23,24] perspectives.

It is indicated that a neural region may be coupled with different networks dynamically,[25,26] and Seitzman et al. provide further neurobiological interpretations of network variants that a single cortical area contains various neurons coding for different stimuli.[27]

[1]College of Intelligence Science and Technology, National University of Defense Technology, Changsha, Hunan 410073, China
[2]Defense Innovation Institute, Academy of Military Sciences (AMS), Beijing 100071, China
[3]Tianjin Artificial Intelligence Innovation Center (TAIIC), Tianjin 300450, China
[4]Lead contact
*Correspondence: dwhu@nudt.edu.cn
https://doi.org/10.1016/j.isci.2024.109206

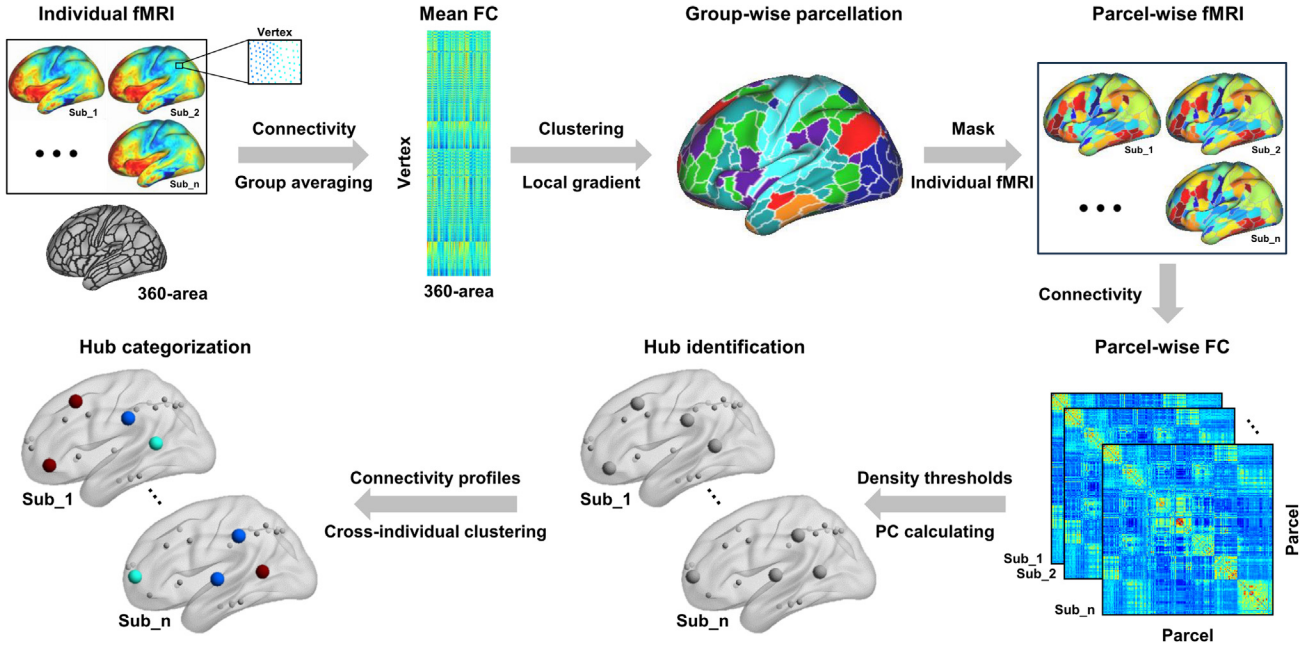

Figure 1. A framework of parcellation and graph theory analysis of the functional human brain

The cerebral cortex was first parcellated based on group-average FC matrix between cortical vertices and 360-area using rs-fMRI, and then we set the group-wise parcellation as template to calculate individual parcel-wise functional connectivity. Each parcel-wise FC matrix was thresholded at a range of graph densities and hubs were identified based on average PC percentile values on individual level, after that, hubs were clustered according to their connectivity profiles across individuals.

Frequency-specific studies of fMRI have attracted much interest. Wang et al. find the frequency-dependent functional separation of the right anterior insula by segregating it into dorsal and ventral parts at slow 6 to slow 3 frequency bands.[28] Sasai et al. find the band-specific shifts of the brain-wide neural coherence and that modules showing the highest variance are in the parieto-occipital regions at 0.01–0.15 Hz.[29] Ries et al. indicate the frequency-dependent alterations of brain intrinsic functional connectivity in major depressive disorder patients.[30]

Previous fMRI studies have confirmed that the static brain networks contain diverse functional systems, namely groups of networks interconnected by different connector hub sets.[31–33] Considering the frequency multiplexing scheme of the cortical networking,[18] we further hypothesize that a single cortical area may participate in various networks simultaneously in different frequency bands, and that the functional systems observed from the frequency perspective might be slightly different compared to the standard static ones, reflecting frequency-specific segregation and integration patterns of the functional human brain.

In this study, using 7T rs-fMRI data from the Human Connectome Project (HCP), we conducted a frequency-specific topology analysis of the functional human brain. Considering that brain topography had direct impact on its topology,[34] we conducted, to our knowledge, the first frequency-specific functional parcellation of the human brain using rs-fMRI. Functional network definition was slightly different across frequencies, which was validated by task activations. A functional atlas was incidentally proposed based on all these frequency-specific parcellations and was validated by stereo-EEG. We found two hub sets existing in both static and frequency-specific networks, and found a cognitive control hub set additionally from a frequency perspective. These three hub sets occupied different positions of the cerebral cortex, they were differentially activated during task performance, and they affected networks differently when being artificially removed. Test-retest experiment on 3T rs-fMRI data confirmed our findings. Moreover, the cognitive control hub could not be derived based on canonical 7 or 17 networks from Yeo et al.,[2] implying its subtlety and the necessity of precise parcellation before exploring frequency-specific topology of the functional human brain.

RESULTS

Parcellation of the human cerebral cortex

The framework of this study is shown in Figure 1. Frequency-specific functional parcellations were first conducted. As shown in Figure 2A and Table 1, the number of obtained networks illustrated a decreasing trend as frequency increased. We found segregated visual network (central and peripheral Vis) at 0.01 Hz, and segregated frontoparietal control network (FPN) (left [lFPN] and right FPN [rFPN]) at 0.02–0.08 Hz. The presence of these two lateralized FPN subnetworks was reported previously,[35–37] although they were rarely detected by whole-brain parcellation. Moreover, the parietal memory network (PMN) existed only in the low-frequency band (0.01–0.02 Hz) and was mainly integrated into

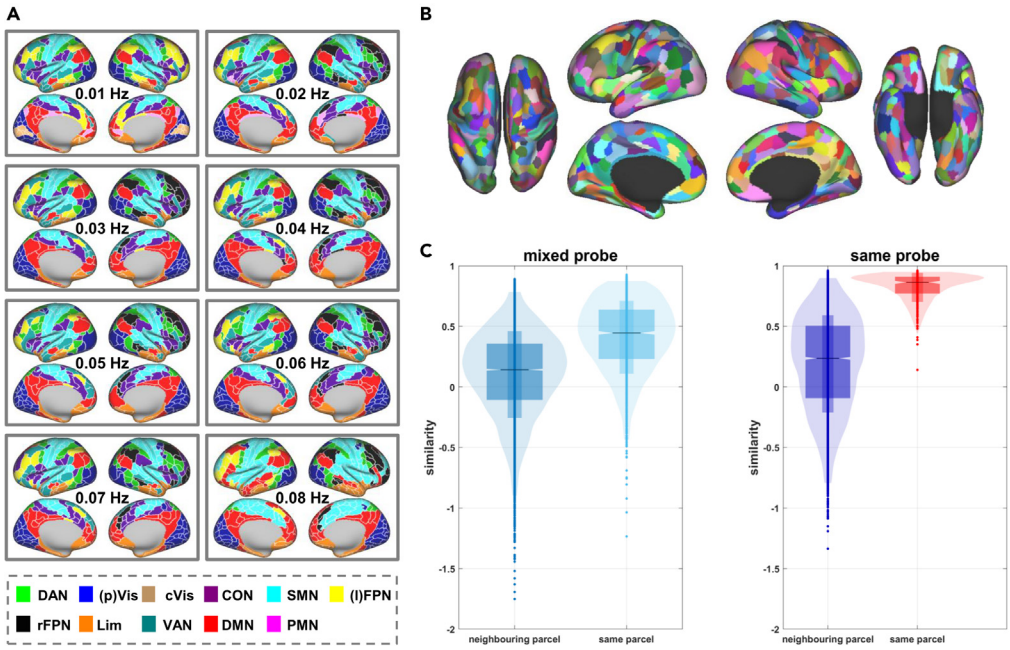

Figure 2. Frequency-specific parcellations and an intrinsic functional atlas

(A) Parcellations across frequencies, with parcel boundaries overlaid.

(B) Intrinsic functional atlas with 456 parcels derived from all frequency-specific parcellations.

(C) The power spectra similarity of stereo-EEG between channels within the same parcel was higher than those in neighboring parcels (left panel), and much higher when we only compared channels in the same probe of the same patient (right panel). $p < 10^{-10}$, two-sample t test.

the default-mode network (DMN) later. The cingulo-opercular network (CON) was integrated into the sensory-motor network (SMN) and the ventral attention network (VAN) merged with DMN at 0.08 Hz. Compared with the static network (Figure S1B), the fronto-limbic network (fLim) and occipito-limbic network were merged, and the dorsal attention network (DAN) and FPN were separated in the frequency-specific networks. Details about the spatial overlap of networks between static and frequency-specific parcellations can be seen in Figure S2. Bilateral symmetry was high at 0.01 Hz (SI = 82.47%), and reduced (SI ≈ 75%) because of the left-right division of FPN afterward. Meanwhile, a Vis region kept stable in the lateral parietal cortex. Parcellation repeatability is shown in Figure S3.

Notably, relationships between networks across situation were not simple integration or segregation. For example, the entire occipital lobe belonged to Vis (0.02–0.08 Hz) or its sub-networks (cVis & pVis, 0.01 Hz). While in the static parcellation, the central parcel of the occipital lobe was a part of fLim, although it was surrounded by Vis. These three division types of the occipital lobe were verified by task activations (Figure S4). To demonstrate that frequency-specific networks were derived by intrinsic frequency-specific FC instead of cluster number, we obtained 7–16 static networks using k-means clustering, similar to Yeo et al.[2] As shown in Figure S5, no matter how many static networks we identified, cVis (which occurred only at 0.01 Hz) was not obtained.

Cortical parcels were created when we applied the watershed edge detection technique to the boundary map. The whole cerebral cortex was divided into ~400 parcels in each frequency band (Figures 2A; Table 1). Based on this, an intrinsic functional atlas was acquired according to the probability of each vertex falling in the same parcel across frequencies, following the practice of Yan et al.[18] As shown in Figure 2B, the atlas had a total of 456 parcels, with 233 parcels in the left hemisphere and 223 in the right. Stereo-EEG was used to verify the plausibility of the proposed atlas (Figure 2C). As we expected, the power spectra similarity between EEG channels within the same parcel was significantly higher than those in neighboring parcels (mean ± SD: 0.41 ± 0.30 vs. 0.10 ± 0.36), and much higher when we only compared channels in the same probe of the same patient (0.82 ± 0.12 vs. 0.19 ± 0.40). Similar results were obtained when we conducted comparisons of EEGs with an excluding criterion of 5 mm (1,620 contacts, mixed probe: 0.39 ± 0.29 vs. 0.10 ± 0.36; same probe: 0.81 ± 0.13 vs. 0.19 ± 0.40) or no exclusion (1,772 contacts, mixed probe: 0.39 ± 0.29 vs. 0.10 ± 0.36; same probe: 0.81 ± 0.13 vs. 0.19 ± 0.40), or when comparisons were conducted in alpha (8–13 Hz), beta (13–30 Hz), and gamma (30–50 Hz) rhythms[38,39] (Figure S6). All the aforementioned comparisons passed the two-sample t test with $p < 10^{-10}$.

Hub identification and categorization

We then calculated the participation coefficient (PC) values of parcels at the individual level and converted them to percentiles, and parcels with the 80th+ percentile of PC values in each individual were regarded as connector hubs. Clustering revealed that two types of connector hubs existed in both static and frequency-specific networks (Figure 3). The first hub set exhibited strong connectivity with

Table 1. Number of networks and parcels of parcellations across frequencies

	Networks	Left parcels	Right parcels
0.01 Hz	10	201	190
0.02 Hz	10	204	203
0.03 Hz	9	205	204
0.04 Hz	9	205	216
0.05 Hz	9	209	208
0.06 Hz	9	204	211
0.07 Hz	9	210	217
0.08 Hz	7	218	211

DAN, Vis, CON, and SMN, while the second showed relatively strong connectivity with VAN and DMN. The network connectivities of these two hub sets roughly illustrated task-positive vs. task-negative[31,40] or extrinsic vs. intrinsic[41] patterns, which were consistent with the hierarchical organization of the resting-state networks.[42] We thus named them task-positive and task-negative hubs, respectively. More importantly, another hub set was observed additionally in the frequency-specific networks at 0.02–0.04 Hz and 0.07 Hz (Figure 3). As they showed strong connectivity with lFPN and rFPN, we called them cognitive control hubs as inspired by Zanto and Gazzaley.[25] Task-positive hubs occupied a majority across all situations. Additional analysis using different PC percentile thresholds revealed identical results (Figure S7).

We converted hub densities to percentiles for normalization, and averaged them cross frequencies containing three sets of hubs (namely 0.02–0.04 Hz and 0.07 Hz). Vertices with the 80^{th}+ percentile average density values were regarded as typical frequency-specific hub sets. As shown in Figure 4A, the task-positive hubs mainly located in anterior intraParietal area, frontal eye fields, Area 5m ventral, Dorsal Area 24d, right Area PF Complex, Medial Area 7A, Area 7PC, and Area Lateral IntraParietal ventral; the task-negative hubs mainly located in Area 9 Middle, Area PGi, and Area 8Av; the cognitive control hubs mainly located in Area 8BM, Area PFm Complex, Area posterior 9-46v, and Area IntraParietal 1. Parcel names were from Glasser et al.[43] for a precise description of hub positions. Group-average task activation maps of 997 subjects from HCP_S1200 were used to measure the task activation similarities of vertices in the hub areas. Specifically, 86 coactivation patterns were obtained during 7 task performance (emotion, gambling, language, motor, relational, social, and working memory), and details of the task-fMRI in HCP could be seen in the study by Barch et al.[44] Pearson's correlation coefficient of group-average task activation z-values (86 dimensions) among vertices was calculated to measure the activation similarities. As shown in Figures 4B and 4C, task activation similarities within the same hub sets were statistically higher than that between different hub sets ($p < 10^{-10}$, two-sample t test). When we averaged the absolute task activation z_values of hub regions in each task, we found that the task-positive hub regions activated for motor and social tasks, and the cognitive control hub regions activated for working memory, language, and relational tasks, while the task-negative hub regions deactivated during all tasks (Figure S8).

Test-retest experiment

Test-retest experiments were conducted on Cohort 2 using templates from Cohort 1, and results are shown in Figures 3 and S9. It can be seen that the categories, proportions, and network connectivity patterns of hubs as well as spatial distributions of the PC percentile values are highly consistent across cohorts. Slight differences can be seen at 0.04 and 0.07 Hz, where task-positive hubs are consistent while two other sets of hubs of Cohort 1 seem to combine together on Cohort 2, which implies that cognitive control hubs are subtle. The test-retest experiment confirms the stabilities of the hub sets and their connectivity profiles.

Hub sets and their connectivity profiles based on templates of RSN_7_400 and RSN_17_400 are shown in Figure S10. Task-positive and task-negative hubs were found on both RSN_7_400 and RSN_17_400, and they showed good stability on proportions and connectivity profiles at the static situation across cohorts. RSN_7_400 illustrated a larger proportion of task-positive hubs and relatively poor stability across cohorts in some frequency bands. Possibly benefitting from a more refined network division, RSN_17_400 showed a more balanced proportion between hub sets and better stability across cohorts in all frequency bands. Notably, the cognitive control hub never appeared in any frequency band, implying the importance of precise topography in topology exploring of the functional human brain.

Effects of hub removal on network structure

We examined how removing a specific hub set would affect the brain's network structure, following the practice of Gordon et al.[32] Considering that the functional network structure had high cross-cohort reproducibility on hub proportion and network connectivity patterns at 0.02 Hz, network structure changes at 0.02 Hz were explored as an example. Removal of the same number of random non-hubs was conducted as a control, and path length metric[45] was used to evaluate brain network structure changes, as removing nodes would inevitably increase network isolation (i.e., increase path lengths), and removing a specific set of hubs would theoretically increase larger path length on specific networks than removal of number-matched non-hubs. Calculation of path length was conducted on binarized connectivity matrices and averaged across graph density thresholds, and paths from disconnected nodes were assigned the maximum distance in the brain before

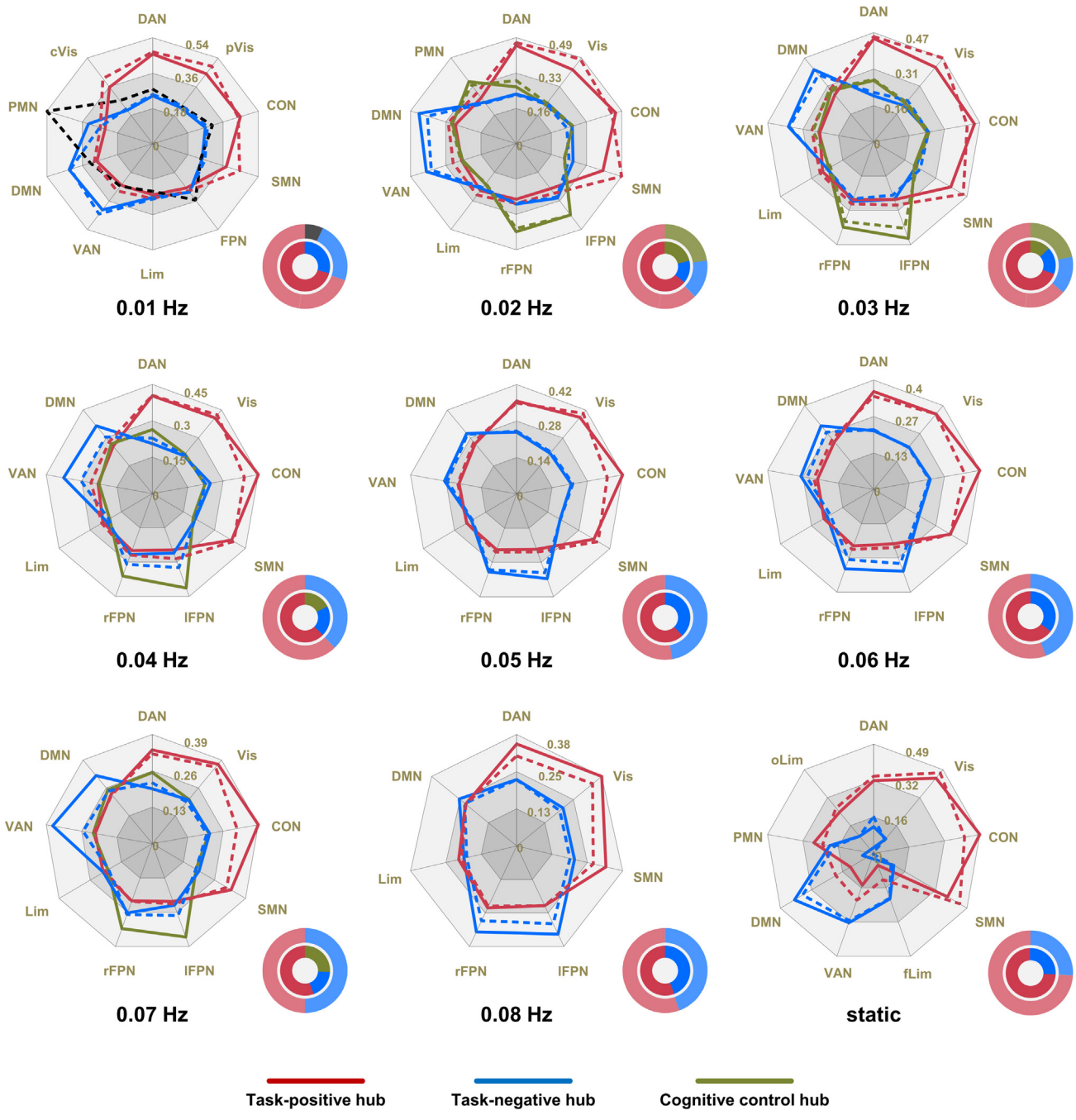

Figure 3. Average network connectivity of each hub set and reproducibility across cohorts

Except for 0.01, 0.04, and 0.07 Hz, hub sets were consistent between Cohort 2 (dotted line) and Cohort 1 (solid line) in cluster number and network connectivity patterns. Pie charts represent the relative ratio of hub sets with corresponding colors, with Cohort 1 inside (dark colors) and Cohort 2 outside (light colors).

removing nodes to avoid infinite values. Results of path lengths after non-hubs removal were averaged across 100 iterations of random non-hub selections. Comparisons between path lengths after hub and non-hub removal were conducted using two-sample t tests, and significance tests were false discovery rate corrected.

Figure 5 shows the effects of removing each hub set from the network, as implemented in Gephi. A single run (Subject ID: 102816, REST3) was selected to show the effects of hub removal on the individual network, as it contained a proper proportion of hub sets (Figure 5B). Compared with the original network structure (Figure 5A), removing task-positive hubs separated CON, DAN, and SMN (Figure 5C). Removal of task-negative hubs separated DMN and VAN (Figure 5E), and removal of cognitive control hubs isolated lFPN and

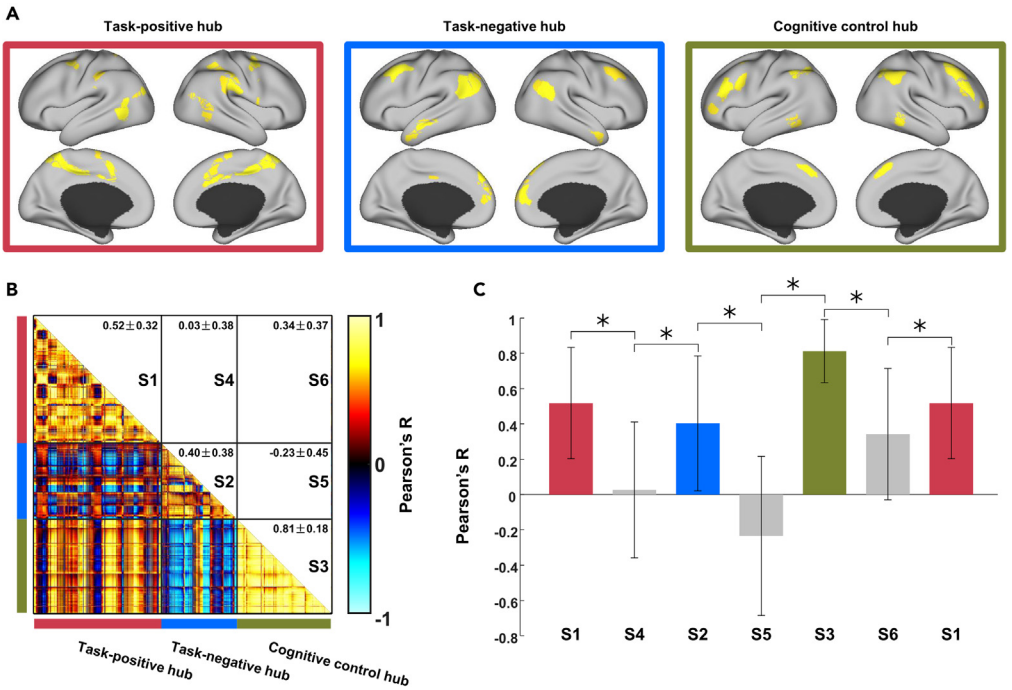

Figure 4. Spatial distributions and task-activation similarity of frequency-specific hubs

(A) Spatial distributions of frequency-specific hub regions. The border color indicates the hub set.

(B) A vertex×vertex matrix illustrating the similarity of task activation between and within hub regions. The line color indicates the hub set. Lower triangle: paired task-activation similarities between vertices. Upper triangle: the labels (S1-S6) and the mean ± standard deviation values of the corresponding regions in the lower triangle.

(C) Between-bub task-activation similarities are lower than the within-hub ones of corresponding two hub regions with significance. Bar represents mean and error bar represents standard deviation. *, $p < 10^{-10}$, two-sample t test.

rFPN (Figure 5G). Compared with random removal of non-hubs across subjects, removing task-positive hubs markedly increased the intra-network path lengths for CON and DAN and the inter-network path lengths between CON and SMN/Vis, DAN, and SMN/CON/Vis (Figure 5D). Removal of task-negative hubs observably increased the intra-network path lengths for DMN and the inter-network path lengths between DMN and VAN (Figure 5F), and removal of cognitive control hubs remarkably increased the intra-network path lengths for lFPN and rFPN and the inter-network path lengths between lFPN and PMN/rFPN/DMN, rFPN, and PMN/CON/DMN (Figure 5H). These results indicated that the removal of different hub sets had different effects on the frequency-specific network organization.

Hub removal had consistent effects across frequency-specific and static networks (Figure S11).

DISCUSSION

Topology as well as hub analysis has been widely conducted in fMRI/MEG/EEG studies to explore the frequency-specific integration/segregation properties of the functional human brain. Most topology studies of functional human brain focus on the quantization of functional integration/segregation. For example, Sasai et al.[46] find different modularity and global efficiencies between very low-frequency band (0.01–0.03 Hz) and low-frequency band (0.07–0.09 Hz) using rs-fMRI data. Schoonheim et al.[47] report increased path length and clustering coefficient in the lower α band in multiple sclerosis patients using resting-state MEG data. Utianski et al.[48] report higher modularity in α band in dementia group compared with cognitively normal group among Parkinson's disease patients using EEG data. Meanwhile, most hub studies focus on the change of hub areas. For example, Hipp et al.[15] and de Pasquale et al.[49] find that MEG-localized hubs depended on the underlying carrier frequency. Ries et al.[30] report frequency-dependent spatial distribution of rs-fMRI-localized hubs. Hatlestad-Hall et al.[50] find that the left central region and the left parietal lateral surface displayed a shift toward greater α band hubness in focal epilepsy patients using EEG data. However, treating the hubs as belonging to a single category may limit the effect of investigations.

In this study, we analyzed the frequency-specific topography and topological organization of the functional human brain using rs-fMRI. We found various frequency-specific neural couplings of the human brain via hub sets, whose reproducibility and plausibility were validated by resting-state and task-related fMRI analysis. Our study may provide a new perspective to the understanding of functional human brain dynamics. Detailed discussions are as follows.

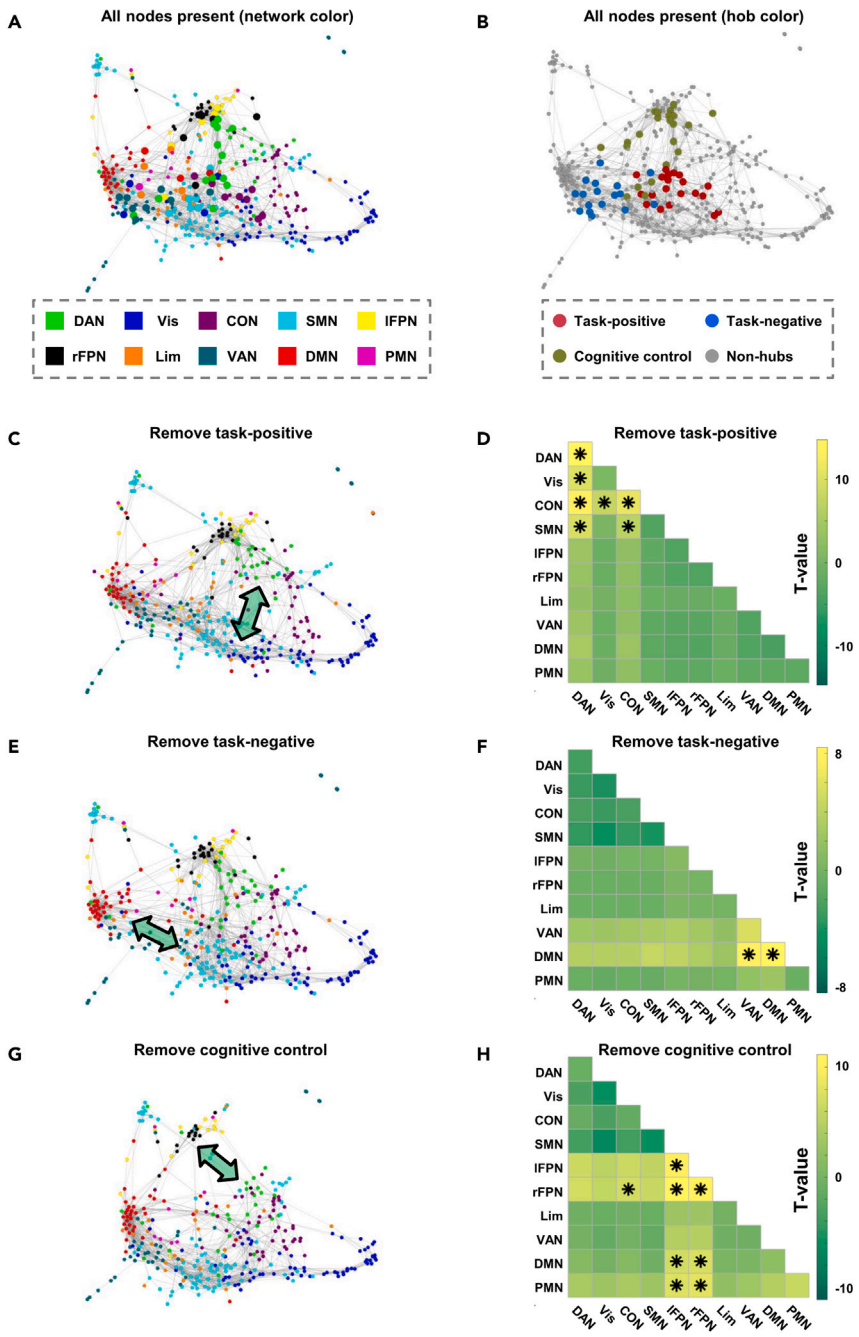

Figure 5. Removing hub sets alters network structure

(A and B) Spring embedding plot of network organization of a single subject at a 3% graph density (Subject ID: 102816, session: REST3, frequency: 0.02 Hz). Hubs are enlarged and colored based on network identities (A) or hub sets (B).

(C, E, and G) Network structures after removing task-positive (C), task-negative (E), and cognitive control (G) hub nodes. Arrows indicate network structure changes; the nodes with a degree of 0 are not displayed.

(D, F, and H) Average path-length changes across subjects after removing task-positive (D), task-negative (F), and cognitive control (H) hubs compared with removal of random non-hubs. *, $p < 10^{-10}$, two-sample t test, FDR-corrected.

Frequency specificity of the functional parcellation

Previously, parcellation based on static FC is the mainstream of resting-state functional parcellation,[3,7,51–60] supplemented by dynamic FC.[61,62] In traditional static parcellations, small networks can be derived by changing cluster number or sparsity of the FC matrix, and

subnetworks can be derived from further subdivisions of large-scale networks.[63] Nevertheless, the dynamic nature of brain networks cannot be revealed by static parcellation. While for parcellation using dynamic FC, there remain important concerns like selecting appropriate parameters and validating the approach.[64] As far as we know, there is no fMRI study on the functional parcellation of human brain from the perspective of frequency. Our research shows that functional networks are frequency specific, and the correspondence between functional subdivisions and task activations provides new insights into brain dynamics.

Topography is vital for exploring brain network topology

Considering the influence of community definition on network topology delineation, it is worthwhile to discuss the selection of network templates when exploring the network topology of the functional human brain. At present, there are two popular strategies for community selection. The one is community detection.[29,32,46,63,65] Nevertheless, the accurate detection of community remains an open problem.[66] The other is the usage of canonical networks or functional atlas as communities.[67–69] It is preferable to use canonical static networks as communities to explore static network topology, but when we explore frequency-specific network topology using static networks, distortions might appear.[70–72]

In this study, we used the widely used static network templates RSN_7 and RSN_17,[2] to see if the delineation of network topology was independent of community definition and if frequency-specific network topology could be distorted using static network templates. Results indicated that the task-positive and task-negative hubs constantly existed in the static networks, whenever the number of networks was 7, 9, or 17, implying the robustness of the static network topology to a certain degree. But the cognitive control hubs were not derived when these canonical static network templates were used for community definition in frequency-specific networks, emphasizing the importance of frequency-specific functional parcellations before exploring frequency-specific network topologies.

Cognitive control hubs are subtle but important

In the functional human brain, a connector hub cannot have strong functional connectivities with all networks. There should be differences in the network connectivity patterns of different connector hubs, which are rarely noticed before.[32] Categorization of the connector hubs helps to understand the segregation and integration of the functional human brain more intuitively. In this study, we observed stable frequency-specific clustering of connector hubs and depicted their functional connectivities with intrinsic networks. This is of pivotal importance for us to better understand how cortical areas work together at different frequencies.

Although we identified the cognitive control hubs in limited frequency bands and with pure data-driven frequency-specific networks, and their reproducibility rates were lower than two other hub sets, they did show hub properties as they were defined with high PC values and they increased network path length more significantly than non-hubs when being removed. Moreover, the cognitive control hubs differed from two other hub sets in spatial distributions, connectivity profiles, task activations, and effects on network topology after removal. The decreases of networks and hub types with the increase of frequency accord with the opinion that the human brain has a higher capacity for information segregation in lower frequency,[46] and considering that hub regions activated differently across tasks (see Figure S8 and Demeter et al[33]), the additional system emerging from the frequency-dependent analysis supports the idea that task modulation of human brain functional networks is frequency specific.[29]

Strategy of frequency division

In this study, we focused the scope of our study on the topography and topology difference of the functional human brain between different frequency bands, so we used the traditionally considered frequency range of BOLD rs-fMRI signal oscillations (0.01–0.08 Hz) and referred to an idea of splitting it into eight equal frequency bands for the compromise of power spectrum resolution and power estimation variance.[73] Nevertheless, although we found topography and topological difference of intrinsic networks among frequency bands, the estimation variance of coherence is related to frequency resolution,[74] which may in part explain the inconsistencies of hub sets in 0.01, 0.04, and 0.07 Hz (another reason may be that the two datasets have different signal-to-noise ratios). The similarities of network topology between some neighboring frequency bands and the instabilities between cohorts might imply that a more scientific and reasonable frequency division strategy is needed in future research, and readers are encouraged to explore topological structures of the functional human brain under different frequency division strategies if interested.

Potential applications

The existence of frequency-specific networks and hubs may provide us with new ideas in clinical neuroscience like non-invasive brain stimulation. Frequency-dependent disruptions of functional brain connectomes in various brain diseases have been reported,[75,76] and studies have indicated that hubs may be ideal targets for transcranial magnetic stimulation (TMS).[77] Moreover, it has been mentioned hard to explain when TMS with different frequencies caused opposite changes of brain activity in a distal area belonging to the same canonical brain network of the stimulated area.[78] Our findings may provide prospective recommendations on TMS parameters like frequency and target location, as well as provide a candidate explanation for TMS-induced changes in the functional human brain.

Limitations of the study

We noticed some shortcomings in this work. First, parcel creation is somewhat subjective. Subjectivity has always been a difficult point in functional parcellation. Although we have avoided parameter selection during network parcellation and thereby avoiding subjectivity to the

greatest extent, when local parcellations were conducted, the edge density threshold which decided the boundary of parcels was selected empirically. Although this is a general approach based on gradient subdivision,[7,31,32] it indeed affected the final parcellation results. Second, we focus on the differences in functional network topology at different frequencies in this study, so the group-wise parcellation is used as the template. However, differences in individual brain functions have attracted increasing attention,[27,79] and it is necessary to consider individual differences in the future.

STAR★METHODS

Detailed methods are provided in the online version of this paper and include the following:

- KEY RESOURCES TABLE
- RESOURCE AVAILABILITY
  - Lead contact
  - Material availability
  - Data and code availability
- EXPERIMENTAL MODEL AND STUDY PARTICIPANTS DETAILS
- METHOD DETAILS
  - Data acquisition and preprocessing
  - Frequency-specific parcellation of the human cerebral cortex
  - Hub identification and categorization
  - Test-retest experiment
- QUANTIFICATION AND STATISTICAL ANALYSIS

SUPPLEMENTAL INFORMATION

Supplemental information can be found online at https://doi.org/10.1016/j.isci.2024.109206.

ACKNOWLEDGMENTS

This work was supported by the National Natural Science Foundation of China (62036013, 61722313, 61773391, 61703407, and 62076250).

AUTHOR CONTRIBUTIONS

Conceptualization, D.H.; data processing, Z.L. and L.P.; formal analysis and visualization, Z.L., J.S., and L.-L.Z.; methodology, Z.L., H.S., and E.Y.; software, Z.L.; writing – original draft, Z.L.; supervision, D.H. and Y.Y.

DECLARATION OF INTERESTS

The authors declare no competing interests.

Received: July 31, 2023
Revised: November 24, 2023
Accepted: February 7, 2024
Published: February 19, 2024

REFERENCES

1. Smith, S.M., Beckmann, C.F., Andersson, J., Auerbach, E.J., Bijsterbosch, J., Douaud, G., Duff, E., Feinberg, D.A., Griffanti, L., Harms, M.P., et al. (2013). Resting-state fMRI in the Human Connectome Project. Neuroimage *80*, 144–168. https://doi.org/10.1016/j.neuroimage.2013.05.039.
2. Yeo, B.T.T., Krienen, F.M., Sepulcre, J., Sabuncu, M.R., Lashkari, D., Hollinshead, M., Roffman, J.L., Smoller, J.W., Zöllei, L., Polimeni, J.R., et al. (2011). The organization of the human cerebral cortex estimated by intrinsic functional connectivity. J. Neurophysiol. *106*, 1125–1165. https://doi.org/10.1152/jn.00338.2011.
3. Shen, X., Tokoglu, F., Papademetris, X., and Constable, R.T. (2013). Groupwise whole-brain parcellation from resting-state fMRI data for network node identification. Neuroimage *82*, 403–415. https://doi.org/10.1016/j.neuroimage.2013.05.081.
4. Dadi, K., Varoquaux, G., Machlouzarides-Shalit, A., Gorgolewski, K.J., Wassermann, D., Thirion, B., and Mensch, A. (2020). Fine-grain atlases of functional modes for fMRI analysis. Neuroimage *221*, 117126. https://doi.org/10.1016/j.neuroimage.2020.117126.
5. Peng, L., Luo, Z., Zeng, L.-L., Hou, C., Shen, H., Zhou, Z., and Hu, D. (2023). Parcellating the human brain using resting-state dynamic functional connectivity. Cerebr. Cortex *33*, 3575–3590. https://doi.org/10.1093/cercor/bhac293.
6. Beckmann, C.F., DeLuca, M., Devlin, J.T., and Smith, S.M. (2005). Investigations into resting-state connectivity using independent component analysis. Philos. Trans. R. Soc. Lond. B Biol. Sci. *360*, 1001–1013. https://doi.org/10.1098/rstb.2005.1634.
7. Gordon, E.M., Laumann, T.O., Adeyemo, B., Huckins, J.F., Kelley, W.M., and Petersen, S.E. (2016). Generation and Evaluation of a Cortical Area Parcellation from Resting-State Correlations. Cerebr. Cortex *26*, 288–303. https://doi.org/10.1093/cercor/bhu239.
8. Tian, Y., Margulies, D.S., Breakspear, M., and Zalesky, A. (2020). Topographic organization of the human subcortex unveiled with functional connectivity gradients. Nat. Neurosci. *23*, 1421–1432. https://doi.org/10.1038/s41593-020-00711-6.
9. Sporns, O. (2013). Network attributes for segregation and integration in the human brain. Curr. Opin. Neurobiol. *23*, 162–171. https://doi.org/10.1016/j.conb.2012.11.015.

10. Bertolero, M.A., Yeo, B.T.T., and D'Esposito, M. (2015). The modular and integrative functional architecture of the human brain. Proc. Natl. Acad. Sci. USA *112*, E6798–E6807. https://doi.org/10.1073/pnas.1510619112.
11. Gratton, C., Sun, H., and Petersen, S.E. (2018). Control networks and hubs. Psychophysiology *55*, e13032. https://doi.org/10.1111/psyp.13032.
12. Kawabata, K., Bagarinao, E., Watanabe, H., Maesawa, S., Mori, D., Hara, K., Ohdake, R., Masuda, M., Ogura, A., Kato, T., et al. (2021). Bridging large-scale cortical networks: Integrative and function-specific hubs in the thalamus. iScience *24*, 103106. https://doi.org/10.1016/j.isci.2021.103106.
13. Hillebrand, A., Tewarie, P., van Dellen, E., Yu, M., Carbo, E.W.S., Douw, L., Gouw, A.A., van Straaten, E.C.W., and Stam, C.J. (2016). Direction of information flow in large-scale resting-state networks is frequency-dependent. Proc. Natl. Acad. Sci. USA *113*, 3867–3872. https://doi.org/10.1073/pnas.1515657113.
14. Brookes, M.J., Woolrich, M., Luckhoo, H., Price, D., Hale, J.R., Stephenson, M.C., Barnes, G.R., Smith, S.M., and Morris, P.G. (2011). Investigating the electrophysiological basis of resting state networks using magnetoencephalography. Proc. Natl. Acad. Sci. USA *108*, 16783–16788. https://doi.org/10.1073/pnas.1112685108.
15. Hipp, J.F., Hawellek, D.J., Corbetta, M., Siegel, M., and Engel, A.K. (2012). Large-scale cortical correlation structure of spontaneous oscillatory activity. Nat. Neurosci. *15*, 884–890. https://doi.org/10.1038/nn.3101.
16. Li, C., Li, P., Zhang, Y., Li, N., Si, Y., Li, F., Cao, Z., Chen, H., Chen, B., Yao, D., and Xu, P. (2024). Effective Emotion Recognition by Learning Discriminative Graph Topologies in EEG Brain Networks. IEEE Transact. Neural Networks Learn. Syst. 1–15. https://doi.org/10.1109/TNNLS.2023.3238519.
17. van Lutterveld, R., van Dellen, E., Pal, P., Yang, H., Stam, C.J., and Brewer, J. (2017). Meditation is associated with increased brain network integration. Neuroimage *158*, 18–25. https://doi.org/10.1016/j.neuroimage.2017.06.071.
18. Yan, Y., Qian, T., Xu, X., Han, H., Ling, Z., Zhou, W., Liu, H., and Hong, B. (2020). Human cortical networking by probabilistic and frequency-specific coupling. Neuroimage *207*, 116363. https://doi.org/10.1016/j.neuroimage.2019.116363.
19. Preti, M.G., Bolton, T.A., and Van De Ville, D. (2017). The dynamic functional connectome: State-of-the-art and perspectives. Neuroimage *160*, 41–54. https://doi.org/10.1016/j.neuroimage.2016.12.061.
20. Buzsáki, G., and Draguhn, A. (2004). Neuronal Oscillations in Cortical Networks. Science *304*, 1926–1929. https://doi.org/10.1126/science.1099745.
21. Shafiei, G., Baillet, S., and Misic, B. (2022). Human electromagnetic and haemodynamic networks systematically converge in unimodal cortex and diverge in transmodal cortex. PLoS Biol. *20*, e3001735. https://doi.org/10.1371/journal.pbio.3001735.
22. Shen, H., Li, Z., Qin, J., Liu, Q., Wang, L., Zeng, L.-L., Li, H., and Hu, D. (2016). Changes in functional connectivity dynamics associated with vigilance network in taxi drivers. Neuroimage *124*, 367–378. https://doi.org/10.1016/j.neuroimage.2015.09.010.
23. Sun, F.T., Miller, L.M., and D'Esposito, M. (2004). Measuring interregional functional connectivity using coherence and partial coherence analyses of fMRI data. Neuroimage *21*, 647–658. https://doi.org/10.1016/j.neuroimage.2003.09.056.
24. Sato, J.R., Takahashi, D.Y., Arcuri, S.M., Sameshima, K., Morettin, P.A., and Baccalá, L.A. (2009). Frequency domain connectivity identification: An application of partial directed coherence in fMRI. Hum. Brain Mapp. *30*, 452–461. https://doi.org/10.1002/hbm.20513.
25. Zanto, T.P., and Gazzaley, A. (2013). Fronto-parietal network: flexible hub of cognitive control. Trends Cognit. Sci. *17*, 602–603. https://doi.org/10.1016/j.tics.2013.10.001.
26. Braga, R.M., and Buckner, R.L. (2017). Parallel Interdigitated Distributed Networks within the Individual Estimated by Intrinsic Functional Connectivity. Neuron *95*, 457–471.e5. https://doi.org/10.1016/j.neuron.2017.06.038.
27. Seitzman, B.A., Gratton, C., Laumann, T.O., Gordon, E.M., Adeyemo, B., Dworetsky, A., Kraus, B.T., Gilmore, A.W., Berg, J.J., Ortega, M., et al. (2019). Trait-like variants in human functional brain networks. Proc. Natl. Acad. Sci. USA *116*, 22851–22861. https://doi.org/10.1073/pnas.1902932116.
28. Wang, Y., Zhu, L., Zou, Q., Cui, Q., Liao, W., Duan, X., Biswal, B., and Chen, H. (2018). Frequency dependent hub role of the dorsal and ventral right anterior insula. Neuroimage *165*, 112–117. https://doi.org/10.1016/j.neuroimage.2017.10.004.
29. Sasai, S., Koike, T., Sugawara, S.K., Hamano, Y.H., Sumiya, M., Okazaki, S., Takahashi, H.K., Taga, G., and Sadato, N. (2021). Frequency-specific task modulation of human brain functional networks: A fast fMRI study. Neuroimage *224*, 117375. https://doi.org/10.1016/j.neuroimage.2020.117375.
30. Ries, A., Hollander, M., Glim, S., Meng, C., Sorg, C., and Wohlschläger, A. (2019). Frequency-Dependent Spatial Distribution of Functional Hubs in the Human Brain and Alterations in Major Depressive Disorder. Front. Hum. Neurosci. *13*, 146.
31. Power, J.D., Cohen, A.L., Nelson, S.M., Wig, G.S., Barnes, K.A., Church, J.A., Vogel, A.C., Laumann, T.O., Miezin, F.M., Schlaggar, B.L., and Petersen, S.E. (2011). Functional Network Organization of the Human Brain. Neuron *72*, 665–678. https://doi.org/10.1016/j.neuron.2011.09.006.
32. Gordon, E.M., Lynch, C.J., Gratton, C., Laumann, T.O., Gilmore, A.W., Greene, D.J., Ortega, M., Nguyen, A.L., Schlaggar, B.L., Petersen, S.E., et al. (2018). Three Distinct Sets of Connector Hubs Integrate Human Brain Function. Cell Rep. *24*, 1687–1695.e4. https://doi.org/10.1016/j.celrep.2018.07.050.
33. Demeter, D.V., Gordon, E.M., Nugiel, T., Garza, A., Larguinho, T.L., and Church, J.A. (2023). Resting-state cortical hubs in youth organize into four categories. Cell Rep. *42*, 112521. https://doi.org/10.1016/j.celrep.2023.112521.
34. Zhang, J., Scholtens, L.H., Wei, Y., van den Heuvel, M.P., Chanes, L., and Barrett, L.F. (2020). Topography Impacts Topology: Anatomically Central Areas Exhibit a "High-Level Connector" Profile in the Human Cortex. Cerebr. Cortex *30*, 1357–1365. https://doi.org/10.1093/cercor/bhz171.
35. Clewett, D., Luo, S., Hsu, E., Ainslie, G., Mather, M., and Monterosso, J. (2014). Increased functional coupling between the left fronto-parietal network and anterior insula predicts steeper delay discounting in smokers. Hum. Brain Mapp. *35*, 3774–3787. https://doi.org/10.1002/hbm.22436.
36. Chang, X., Shen, H., Wang, L., Liu, Z., Xin, W., Hu, D., and Miao, D. (2014). Altered default mode and fronto-parietal network subsystems in patients with schizophrenia and their unaffected siblings. Brain Res. *1562*, 87–99. https://doi.org/10.1016/j.brainres.2014.03.024.
37. Haupt, M., Ruiz-Rizzo, A.L., Sorg, C., and Finke, K. (2020). Right-lateralized fronto-parietal network and phasic alertness in healthy aging. Sci. Rep. *10*, 4823. https://doi.org/10.1038/s41598-020-61844-z.
38. Leopold, D.A., Murayama, Y., and Logothetis, N.K. (2003). Very Slow Activity Fluctuations in Monkey Visual Cortex: Implications for Functional Brain Imaging. Cerebr. Cortex *13*, 422–433. https://doi.org/10.1093/cercor/13.4.422.
39. Mantini, D., Perrucci, M.G., Del Gratta, C., Romani, G.L., and Corbetta, M. (2007). Electrophysiological signatures of resting state networks in the human brain. Proc. Natl. Acad. Sci. USA *104*, 13170–13175. https://doi.org/10.1073/pnas.0700668104.
40. Fox, M.D., Snyder, A.Z., Vincent, J.L., Corbetta, M., Van Essen, D.C., and Raichle, M.E. (2005). The human brain is intrinsically organized into dynamic, anticorrelated functional networks. Proc. Natl. Acad. Sci. USA *102*, 9673–9678. https://doi.org/10.1073/pnas.0504136102.
41. Doucet, G., Naveau, M., Petit, L., Delcroix, N., Zago, L., Crivello, F., Jobard, G., Tzourio-Mazoyer, N., Mazoyer, B., Mellet, E., and Joliot, M. (2011). Brain activity at rest: a multiscale hierarchical functional organization. J. Neurophysiol. *105*, 2753–2763. https://doi.org/10.1152/jn.00895.2010.
42. Vidaurre, D., Smith, S.M., and Woolrich, M.W. (2017). Brain network dynamics are hierarchically organized in time. Proc. Natl. Acad. Sci. USA *114*, 12827–12832. https://doi.org/10.1073/pnas.1705120114.
43. Glasser, M.F., Coalson, T.S., Robinson, E.C., Hacker, C.D., Harwell, J., Yacoub, E., Ugurbil, K., Andersson, J., Beckmann, C.F., Jenkinson, M., et al. (2016). A multi-modal parcellation of human cerebral cortex. Nature *536*, 171–178. https://doi.org/10.1038/nature18933.
44. Barch, D.M., Burgess, G.C., Harms, M.P., Petersen, S.E., Schlaggar, B.L., Corbetta, M., Glasser, M.F., Curtiss, S., Dixit, S., Feldt, C., et al. (2013). Function in the human connectome: Task-fMRI and individual differences in behavior. Neuroimage *80*, 169–189. https://doi.org/10.1016/j.neuroimage.2013.05.033.
45. Rubinov, M., and Sporns, O. (2010). Complex network measures of brain connectivity: Uses and interpretations. Neuroimage *52*, 1059–1069. https://doi.org/10.1016/j.neuroimage.2009.10.003.
46. Sasai, S., Homae, F., Watanabe, H., Sasaki, A.T., Tanabe, H.C., Sadato, N., and Taga, G. (2014). Frequency-specific network topologies in the resting human brain. Front. Hum. Neurosci. *8*, 1022.
47. Schoonheim, M.M., Geurts, J.J.G., Landi, D., Douw, L., van der Meer, M.L., Vrenken, H., Polman, C.H., Barkhof, F., and Stam, C.J. (2013). Functional connectivity changes in multiple sclerosis patients: A graph analytical study of MEG resting state data. Hum. Brain Mapp. *34*, 52–61. https://doi.org/10.1002/hbm.21424.
48. Utianski, R.L., Caviness, J.N., van Straaten, E.C.W., Beach, T.G., Dugger, B.N., Shill, H.A.,

Driver-Dunckley, E.D., Sabbagh, M.N., Mehta, S., Adler, C.H., and Hentz, J.G. (2016). Graph theory network function in Parkinson's disease assessed with electroencephalography. Clin. Neurophysiol. *127*, 2228–2236. https://doi.org/10.1016/j.clinph.2016.02.017.

49. de Pasquale, F., Spadone, S., Betti, V., Corbetta, M., and Della Penna, S. (2021). Temporal modes of hub synchronization at rest. Neuroimage *235*, 118005. https://doi.org/10.1016/j.neuroimage.2021.118005.
50. Hatlestad-Hall, C., Bruña, R., Syvertsen, M.R., Erichsen, A., Andersson, V., Vecchio, F., Miraglia, F., Rossini, P.M., Renvall, H., Taubøll, E., et al. (2021). Source-level EEG and graph theory reveal widespread functional network alterations in focal epilepsy. Clin. Neurophysiol. *132*, 1663–1676. https://doi.org/10.1016/j.clinph.2021.04.008.
51. Fan, L., Wang, J., Zhang, Y., Han, W., Yu, C., and Jiang, T. (2014). Connectivity-Based Parcellation of the Human Temporal Pole Using Diffusion Tensor Imaging. Cerebr. Cortex *24*, 3365–3378. https://doi.org/10.1093/cercor/bht196.
52. Zhang, Y., Fan, L., Zhang, Y., Wang, J., Zhu, M., Zhang, Y., Yu, C., and Jiang, T. (2014). Connectivity-Based Parcellation of the Human Posteromedial Cortex. Cerebr. Cortex *24*, 719–727. https://doi.org/10.1093/cercor/bhs353.
53. Shi, F., Salzwedel, A.P., Lin, W., Gilmore, J.H., and Gao, W. (2018). Functional Brain Parcellations of the Infant Brain and the Associated Developmental Trends. Cerebr. Cortex *28*, 1358–1368. https://doi.org/10.1093/cercor/bhx062.
54. Barnes, K.A., Nelson, S.M., Cohen, A.L., Power, J.D., Coalson, R.S., Miezin, F.M., Vogel, A.C., Dubis, J.W., Church, J.A., Petersen, S.E., and Schlaggar, B.L. (2012). Parcellation in Left Lateral Parietal Cortex Is Similar in Adults and Children. Cerebr. Cortex *22*, 1148–1158. https://doi.org/10.1093/cercor/bhr189.
55. Schaefer, A., Kong, R., Gordon, E.M., Laumann, T.O., Zuo, X.-N., Holmes, A.J., Eickhoff, S.B., and Yeo, B.T.T. (2018). Local-Global Parcellation of the Human Cerebral Cortex from Intrinsic Functional Connectivity MRI. Cerebr. Cortex *28*, 3095–3114. https://doi.org/10.1093/cercor/bhx179.
56. Craddock, R.C., James, G.A., Holtzheimer, P.E., Iii, Hu, X.P., and Mayberg, H.S. (2012). A whole brain fMRI atlas generated via spatially constrained spectral clustering. Hum. Brain Mapp. *33*, 1914–1928. https://doi.org/10.1002/hbm.21333.
57. Thorsten, K., Luke, J.C., Soyoung, Q.P., Jakob, H., and John-Dylan, H. (2012). Connectivity-Based Parcellation of the Human Orbitofrontal Cortex. J. Neurosci. *32*, 6240. https://doi.org/10.1523/JNEUROSCI.0257-12.2012.
58. Carine, K., Arthur, A., Eric, B., Eric, B., Stéphane, L., and Frédéric, A.B. (2012). Functional Parcellation of the Lateral Mesencephalus. J. Neurosci. *32*, 9396. https://doi.org/10.1523/JNEUROSCI.0509-12.2012.
59. Blumensath, T., Jbabdi, S., Glasser, M.F., Van Essen, D.C., Ugurbil, K., Behrens, T.E.J., and Smith, S.M. (2013). Spatially constrained hierarchical parcellation of the brain with resting-state fMRI. Neuroimage *76*, 313–324. https://doi.org/10.1016/j.neuroimage.2013.03.024.
60. Parisot, S., Arslan, S., Passerat-Palmbach, J., Wells, W.M., and Rueckert, D. (2016). Group-wise parcellation of the cortex through multi-scale spectral clustering. Neuroimage *136*, 68–83. https://doi.org/10.1016/j.neuroimage.2016.05.035.
61. Ji, B., Li, Z., Li, K., Li, L., Langley, J., Shen, H., Nie, S., Zhang, R., and Hu, X. (2016). Dynamic thalamus parcellation from resting-state fMRI data. Hum. Brain Mapp. *37*, 954–967. https://doi.org/10.1002/hbm.23079.
62. Zhong, Q., Xu, H., Qin, J., Zeng, L.-L., Hu, D., and Shen, H. (2019). Functional parcellation of the hippocampus from resting-state dynamic functional connectivity. Brain Res. *1715*, 165–175. https://doi.org/10.1016/j.brainres.2019.03.023.
63. Gordon, E.M., Laumann, T.O., Marek, S., Raut, R.V., Gratton, C., Newbold, D.J., Greene, D.J., Coalson, R.S., Snyder, A.Z., Schlaggar, B.L., et al. (2020). Default-mode network streams for coupling to language and control systems. Proc. Natl. Acad. Sci. USA *117*, 17308–17319. https://doi.org/10.1073/pnas.2005238117.
64. Hutchison, R.M., Womelsdorf, T., Allen, E.A., Bandettini, P.A., Calhoun, V.D., Corbetta, M., Della Penna, S., Duyn, J.H., Glover, G.H., Gonzalez-Castillo, J., et al. (2013). Dynamic functional connectivity: Promise, issues, and interpretations. Neuroimage *80*, 360–378. https://doi.org/10.1016/j.neuroimage.2013.05.079.
65. Gordon, E.M., Laumann, T.O., Gilmore, A.W., Newbold, D.J., Greene, D.J., Berg, J.J., Ortega, M., Hoyt-Drazen, C., Gratton, C., Sun, H., et al. (2017). Precision Functional Mapping of Individual Human Brains. Neuron *95*, 791–807.e7. https://doi.org/10.1016/j.neuron.2017.07.011.
66. Liu, W., Pellegrini, M., and Wang, X. (2014). Detecting Communities Based on Network Topology. Sci. Rep. *4*, 5739. https://doi.org/10.1038/srep05739.
67. Fan, F., Liao, X., Lei, T., Zhao, T., Xia, M., Men, W., Wang, Y., Hu, M., Liu, J., Qin, S., et al. (2021). Development of the default-mode network during childhood and adolescence: A longitudinal resting-state fMRI study. Neuroimage *226*, 117581. https://doi.org/10.1016/j.neuroimage.2020.117581.
68. Hadley, J.A., Kraguljac, N.V., White, D.M., Ver Hoef, L., Tabora, J., and Lahti, A.C. (2016). Change in brain network topology as a function of treatment response in schizophrenia: a longitudinal resting-state fMRI study using graph theory. NPJ Schizophr. *2*, 16014. https://doi.org/10.1038/npjschz.2016.14.
69. Song, K., Li, J., Zhu, Y., Ren, F., Cao, L., and Huang, Z.-G. (2021). Altered Small-World Functional Network Topology in Patients with Optic Neuritis: A Resting-State fMRI Study. Dis. Markers *2021*, 9948751. https://doi.org/10.1155/2021/9948751.
70. Wig, G.S., Schlaggar, B.L., and Petersen, S.E. (2011). Concepts and principles in the analysis of brain networks. Ann. N. Y. Acad. Sci. *1224*, 126–146. https://doi.org/10.1111/j.1749-6632.2010.05947.x.
71. Smith, S.M., Miller, K.L., Salimi-Khorshidi, G., Webster, M., Beckmann, C.F., Nichols, T.E., Ramsey, J.D., and Woolrich, M.W. (2011). Network modelling methods for FMRI. Neuroimage *54*, 875–891. https://doi.org/10.1016/j.neuroimage.2010.08.063.
72. Butts, C.T. (2009). Revisiting the Foundations of Network Analysis. Science *325*, 414–416. https://doi.org/10.1126/science.1171022.
73. Liu, D., Yan, C., Ren, J., Yao, L., Kiviniemi, V.J., and Zang, Y. (2010). Using coherence to measure regional homogeneity of resting-state fMRI signal. Front. Syst. Neurosci. *4*, 24.
74. Zaveri, H.P., Williams, W.J., Sackellares, J.C., Beydoun, A., Duckrow, R.B., and Spencer, S.S. (1999). Measuring the coherence of intracranial electroencephalograms. Clin. Neurophysiol. *110*, 1717–1725. https://doi.org/10.1016/S1388-2457(99)00136-4.
75. Qian, L., Zhang, Y., Zheng, L., Fu, X., Liu, W., Shang, Y., Zhang, Y., Xu, Y., Liu, Y., Zhu, H., and Gao, J.-H. (2017). Frequency specific brain networks in Parkinson's disease and comorbid depression. Brain Imaging Behav. *11*, 224–239. https://doi.org/10.1007/s11682-016-9514-9.
76. Liu, J., Li, M., Pan, Y., Lan, W., Zheng, R., Wu, F.-X., and Wang, J. (2017). Complex Brain Network Analysis and Its Applications to Brain Disorders: A Survey. Complexity *2017*, 8362741. https://doi.org/10.1155/2017/8362741.
77. Lynch, C.J., Breeden, A.L., Gordon, E.M., Cherry, J.B.C., Turkeltaub, P.E., and Vaidya, C.J. (2019). Precision Inhibitory Stimulation of Individual-Specific Cortical Hubs Disrupts Information Processing in Humans. Cerebr. Cortex *29*, 3912–3921. https://doi.org/10.1093/cercor/bhy270.
78. Beynel, L., Powers, J.P., and Appelbaum, L.G. (2020). Effects of repetitive transcranial magnetic stimulation on resting-state connectivity: A systematic review. Neuroimage *211*, 116596. https://doi.org/10.1016/j.neuroimage.2020.116596.
79. Gordon, E.M., Laumann, T.O., Adeyemo, B., Gilmore, A.W., Nelson, S.M., Dosenbach, N.U.F., and Petersen, S.E. (2017). Individual-specific features of brain systems identified with resting state functional correlations. Neuroimage *146*, 918–939. https://doi.org/10.1016/j.neuroimage.2016.08.032.
80. Glasser, M.F., Sotiropoulos, S.N., Wilson, J.A., Coalson, T.S., Fischl, B., Andersson, J.L., Xu, J., Jbabdi, S., Webster, M., Polimeni, J.R., et al. (2013). The minimal preprocessing pipelines for the Human Connectome Project. Neuroimage *80*, 105–124. https://doi.org/10.1016/j.neuroimage.2013.04.127.
81. Vu, An T., Jamison, K., Glasser, M.F., Smith, S.M., Coalson, T., Moeller, S., Auerbach, E.J., Uğurbil, K., and Yacoub, E. (2017). Tradeoffs in pushing the spatial resolution of fMRI for the 7T Human Connectome Project. Neuroimage *154*, 23–32. https://doi.org/10.1016/j.neuroimage.2016.11.049.
82. Thompson, W.H., and Fransson, P. (2015). The frequency dimension of fMRI dynamic connectivity: Network connectivity, functional hubs and integration in the resting brain. Neuroimage *121*, 227–242. https://doi.org/10.1016/j.neuroimage.2015.07.022.
83. Müller, K., Lohmann, G., Bosch, V., and von Cramon, D.Y. (2001). On Multivariate Spectral Analysis of fMRI Time Series. Neuroimage *14*, 347–356. https://doi.org/10.1006/nimg.2001.0804.
84. Curtis, C.E., Sun, F.T., Miller, L.M., and D'Esposito, M. (2005). Coherence between fMRI time-series distinguishes two spatial working memory networks. Neuroimage *26*, 177–183. https://doi.org/10.1016/j.neuroimage.2005.01.040.
85. Thomson, D.J. (1982). Spectrum estimation and harmonic analysis. Proc. IEEE *70*, 1055–1096. https://doi.org/10.1109/PROC.1982.12433.

86. Zhou, C., Zemanová, L., Zamora, G., Hilgetag, C.C., and Kurths, J. (2006). Hierarchical Organization Unveiled by Functional Connectivity in Complex Brain Networks. Phys. Rev. Lett. *97*, 238103. https://doi.org/10.1103/PhysRevLett.97.238103.
87. Luo, Z., Zeng, L.-L., Qin, J., Hou, C., Shen, H., and Hu, D. (2020). Functional Parcellation of Human Brain Precuneus Using Density-Based Clustering. Cerebr. Cortex *30*, 269–282. https://doi.org/10.1093/cercor/bhz086.
88. Belkin, M., and Niyogi, P. (2003). Laplacian Eigenmaps for Dimensionality Reduction and Data Representation. Neural Comput. *15*, 1373–1396. https://doi.org/10.1162/089976603321780317.
89. Rodriguez, A., and Laio, A. (2014). Clustering by fast search and find of density peaks. Science *344*, 1492–1496. https://doi.org/10.1126/science.1242072.
90. Su, J., Shen, H., Peng, L., and Hu, D. (2024). Few-shot domain-adaptive anomaly detection for cross-site brain images. IEEE Trans. Pattern Anal. Mach. Intell. *46*, 1819–1835. https://doi.org/10.1109/TPAMI.2021.3125686.
91. Cohen, A.L., Fair, D.A., Dosenbach, N.U.F., Miezin, F.M., Dierker, D., Van Essen, D.C., Schlaggar, B.L., and Petersen, S.E. (2008). Defining functional areas in individual human brains using resting functional connectivity MRI. Neuroimage *41*, 45–57. https://doi.org/10.1016/j.neuroimage.2008.01.066.
92. Sadaghiani, S., Brookes, M.J., and Baillet, S. (2022). Connectomics of human electrophysiology. Neuroimage *247*, 118788. https://doi.org/10.1016/j.neuroimage.2021.118788.
93. Frauscher, B., von Ellenrieder, N., Zelmann, R., Doležalová, I., Minotti, L., Olivier, A., Hall, J., Hoffmann, D., Nguyen, D.K., Kahane, P., et al. (2018). Atlas of the normal intracranial electroencephalogram: neurophysiological awake activity in different cortical areas. Brain *141*, 1130–1144. https://doi.org/10.1093/brain/awy035.
94. Hacker, C.D., Snyder, A.Z., Pahwa, M., Corbetta, M., and Leuthardt, E.C. (2017). Frequency-specific electrophysiologic correlates of resting state fMRI networks. Neuroimage *149*, 446–457. https://doi.org/10.1016/j.neuroimage.2017.01.054.
95. Su, J., Khoo, H.M., von Ellenrieder, N., Zeng, L.-L., Hu, D., Dubeau, F., and Gotman, J. (2019). fMRI functional connectivity as an indicator of interictal epileptic discharges. Neuroimage. Clin. *24*, 102038. https://doi.org/10.1016/j.nicl.2019.102038.
96. Guimerà, R., and Nunes Amaral, L.A. (2005). Functional cartography of complex metabolic networks. Nature *433*, 895–900. https://doi.org/10.1038/nature03288.
97. Gratton, C., Laumann, T.O., Gordon, E.M., Adeyemo, B., and Petersen, S.E. (2016). Evidence for Two Independent Factors that Modify Brain Networks to Meet Task Goals. Cell Rep. *17*, 1276–1288. https://doi.org/10.1016/j.celrep.2016.10.002.

STAR★METHODS

KEY RESOURCES TABLE

REAGENT or RESOURCE	SOURCE	IDENTIFIER
Deposited data		
HCP CIFTI fMRI data	https://www.humanconnectome.org/study/hcp-young-adult	N/A
Stereo-EEG data	https://mni-open-ieegatlas.research.mcgill.ca	N/A
Software and algorithms		
MATLAB	https://www.mathworks.com	RRID:SCR 001622
Connectome Workbench	https://www.humanconnectome.org/software/connectome-workbench.html	RRID:SCR 008750
Brain connectivity toolbox	http://sites.google.com/site/bctnet/	RRID:SCR 004841
Gephi	https://gephi.org/	RRID:SCR 004293
Gradient parcellation code	https://sites.wustl.edu/petersenschlaggarlab/	N/A

RESOURCE AVAILABILITY

Lead contact

Further information and requests for resources should be directed to and will be fulfilled by the Lead Contact, Dewen Hu (dwhu@nudt.edu.cn)

Material availability

No new materials were generated for this study.

Data and code availability

- HCP CIFTI fMRI data are in https://www.humanconnectome.org/study/hcp-young-adult, and Stereo-EEG data are in https://mni-open-ieegatlas.research.mcgill.ca.
- Gradient parcellation code has been deposited at https://sites.wustl.edu/petersenschlaggarlab/.
- Other items: Parcellation results and the intrinsic functional atlas with 456 parcels are publicly available at https://github.com/luozhuxi/Frequency-parcellation. Any additional information required to reanalyze the data reported in this paper is available from the lead contact upon request.

EXPERIMENTAL MODEL AND STUDY PARTICIPANTS DETAILS

All the data used in this manuscript were obtained from publicly available databases and no new sample collection was performed.

METHOD DETAILS

Data acquisition and preprocessing

All fMRI data are from the HCP Young Adult dataset (age 22–37 years), which are described detailedly in previous studies.[80,81] There are 1086 subjects in the 3T dataset and 184 subjects in the 7T dataset, with 175 subjects undergoing both 3T and 7T fMRI scans. The scanning direction of the 7T fMRI data is AP (anterior-to-posterior)/PA (posterior-to-anterior), which is different from that of 3T fMRI data (LR/RL), and 7T fMRI data greatly improves the signal-to-noise ratio.[81] Both 3T and 7T fMRI data are preprocessed by the standard HCP preprocessing pipelines, including distortion correction and image alignment, projection into the 2 mm standard 32k CIFTI grayordinates space with 59,412 valid cortical surface vertices, removal of nuisance covariates (white matter, cerebrospinal fluid signals, and 24 head motion parameters) with the ICA + FIX approach, and slight smoothing with a 2-mm full-width half-maximum Gaussian kernel.[80] We selected fMRI data with scanning direction of PA in the 7T dataset for parcellation and network topology exploring (182 subjects, 72 males, Cohort 1). 3T fMRI data (runs: REST1_LR, 890 subjects, 421 males, Cohort 2) were used for the test-retest experiment, with no intersection between two cohorts. We removed the first 15 frames of 7T fMRI data (TR = 1 s) and the first 20 frames of 3T fMRI data (TR = 0.72 s) to ensure magnetic saturation, and then performed detrending to regress out linear trends before calculating spectral FC at discrete frequency bands. The fMRI data were further band-pass filtered (0.01–0.08 Hz) to calculate static FC.

Frequency-specific parcellation of the human cerebral cortex

We first conducted group-wise frequency-specific parcellation of the human cerebral cortex. Static parcellation based on static FC was also conducted for comparison. In detail, for each individual, we calculated the static and spectral FC between all 59,412 cortical vertices and the 360 cortical areas from Glasser et al.[43] to obtain one static FC matrix and eight spectral FC matrices, or frequency graphlets,[82] within the frequency range of interest (0.01–0.08 Hz, step = 0.01 Hz). The usage of 360 areas instead of the whole cortical vertices as target ROIs was to improve signal-to-noise ratio.[60] The number of frequency segments was suggested by Liu et al.[73] to balance the frequency resolution of the power spectrum and the variance of power estimation. Pearson's correlation coefficient and spectral coherence were used as measures of static and spectral FC, respectively. The spectral coherence of two time-series x, y at frequency λ is defined as:

$$Coh_{xy}(\lambda) = \frac{\left|f_{xy}(\lambda)\right|^2}{\left|f_{xx}(\lambda)f_{yy}(\lambda)\right|}$$

where $f_{xy}(\lambda)$ is the cross spectrum of x and y, $f_{xx}(\lambda)$ is the power spectrum of x, and $f_{yy}(\lambda)$ is the power spectrum of y.[83,84] We detected the spectrum component using a multi-taper spectrum estimation algorithm.[85] After that, those FC matrices were z-transformed and averaged across individuals. In this way, we obtained nine group-average FC matrices with the dimension of 59,412 × 360 (one correlation matrix and eight frequency graphlets) for parcellation.

Considering the hierarchical organization of the functional human brain,[86] it is difficult to depict global networks and local parcels simultaneously based on FC without any prior knowledge or constraint. In this study, we identified networks and parcels using the global similarity (clustering) and local gradient (abrupt FC changes) method, respectively.

We used our previously proposed eigen-clustering (EIC)[87] method for network parcellation. EIC is composed of Laplacian eigenmaps[88] for dimensionality reduction and data optimization, and density-peaks clustering (DPC)[89] for resisting noise and automatically identifying clustering centroids. We concatenated the Laplacian eigenvectors with dimension of d = 3–15 before DPC referring to the practice of previous studies.[5,61] EIC is parameter-free and has demonstrated its superiority in human brain parcellation.[5,87,90]

Parcel creation was conducted using a gradient-based cortical subdivision algorithm proposed by Cohen et al.[91] We first calculated the similarity matrix by calculating the pairwise spatial correlation of FC among all cortical vertices. For the consistency of the global (network) and local (parcel) parcellation, the functional similarity between vertices was measured as the Pearson's correlation coefficient among the 59,412 concatenated Laplacian eigenvectors (vector dimension: $\sum_{k=3}^{15} k = 117$). For each column of the similarity matrix, we used Connectome Workbench to calculate the first spatial derivative, resulting in 59,412 gradient maps, then the watershed edge detection technique was used on the gradient maps to get 59,412 corresponding boundary maps, and the watershed edge detection technique was used again on the averaged boundary map to identify parcels.

In detail, local minima were defined as vertices with boundary values smaller than their neighbors within 3 vertices, then parcels grew iteratively from those local minima until they met each other. The resulting parcels were then merged based on two metrics.[7,32,65] First, if a parcel contained less than 30 vertices, it would be merged to its neighbor with the minimum median boundary value. Second, neighboring parcels with median boundary value under the 60th percentile of the whole cortical boundary values would be merged to ensure sufficient dissimilarity between parcels. For the utmost correspondence of the global and local parcellations, neighboring parcels were merged only if they were within the same network. In this way, each cortical vertex had a network label and a parcel label.

Considering that intracranial EEG data can assess neural activity directly, it is regarded as a gold standard of functional brain mapping derived from other indirect metabolic signals like BOLD, for that neuros within the same parcel are believed to have similar neural activities.[5,92] Stereo-EEG data from 106 epilepsy patients (years: 33.1 ± 10.8, 54 males) in a multicenter study[93] were used to verify the plausibility of our proposed atlas. These EEG data were acquired from electrode contacts placed in brain regions with normal activities, and were filtered by a 0.5–80 Hz band-pass filter and downsampled to 200 Hz, and 913 contacts were selected from 1772 candidates after excluding those at least 2 mm away from the nearest cortical vertex. Cross-correlation of their power spectra (0.5–80 Hz) was used as an indicator of the similarity between EEG signals collected in each contact, after regressing out inter-contact distance.[94,95]

Hub identification and categorization

Hub identification and categorization were conducted following the practice of Gordon et al.[32] For each individual, the hub region was defined using the participation coefficient (PC) metric. First, the parcel signal was defined as the average time-series among its vertices, and FC among parcels was calculated to create a parcel-wise connectivity matrix. To mitigate the impact of BOLD signal overlap, FC between parcels within the geodetic distance of 15 vertices (about 30 mm) were set to zero.[32,33] We set a series of graph density thresholds[32,33] (0.3%–0.5%, in 0.1% increments; and 0.5%–5%, in 0.5% increments) to retain the largest elements in the matrix. For each thresholded matrix, the PC value of parcel i was calculated as follows:

$$PC_i = 1 - \sum_{m \in M} \left(\frac{K_i(m)}{K_i}\right)^2$$

where M is the set of all networks, K_i is the total number of edges connected to parcel i, namely its parcel degree, and $K_i(m)$ is the number of edges connected to parcel i within network m.[77] Generally speaking, a parcel with low degree might produce a large PC value, but it would not be a candidate hub. Thus, a parcel's PC value was set to zero if its degree was in the bottom quartile.[32,33] A similar operation was to identify

parcels with both high PCs and high within-module z-scores as connector hubs,[96] which can also avoid parcels with low degrees being hubs. After that, PC values were converted to percentiles for normalization and averaged across graph density thresholds for robustness. Parcels with the 80th+ average percentile PC values were defined as connector hubs.[10,32,33,97]

As for hub categorization, we first calculated the average FC between the hub parcel and all parcels outside 30 mm away from it within each network as its network connectivity profile at the individual level,[32] and then hubs were clustered across individuals based on their connectivity profiles using DPC, as it can determine the cluster number automatically and robustly.[89]

Test-retest experiment

Group-wise parcellation repeatability was validated with different target ROIs (1000 parcels[55] vs. 360 parcels; [43] scanning direction (AP vs. PA), or data cohort (Cohort 2 vs. Cohort 1). Boundary similarities were evaluated as overlap between original and contrasted boundary maps after thresholding both at the 60th percentile[7] and quantized as boundary overlap rate (the size of the intersection of two boundaries divided by the size of their union). Network similarities were evaluated and quantized as spatial overlap rate.[87] Test-retest experiment of topological organization was conducted on Cohort 2. We concentrated our attention on the topography and topology difference of functional human brain across frequencies, group-wise parcellation contributed to avoiding the interference of individual topography differences as well as saving computing resources. Moreover, network topology based on the same topography also benefited to comparison between cohorts. For the above reasons, we considered group-wise parcellations of Cohort 1 as templates to calculate individual parcel-wise FC for hub identification and categorization. Considering that brain topography had direct impact on its topology,[34] we conducted the above-mentioned hub identification and categorization operations on the canonical 7 and 17 networks,[2] to see if the frequency-specific parcellations were necessary for precise exploring of network topology. Parcel template was set to 400-area parcellation[55] for rough match of parcel amount. For convenience, we named them RSN_7_400 and RSN_17_400, respectively.

QUANTIFICATION AND STATISTICAL ANALYSIS

Statistical analyses were performed using a two-sample t-test.